Biomass and Bioenergy 99 (2017) 38–48

Contents lists available at ScienceDirect

Biomass and Bioenergy

journal homepage: http://www.elsevier.com/locate/biombioe

Review

Simplified model and simulation of biomass particle suspension combustion in one-dimensional flow applied to bagasse boilers

Germán Navarrete Cereijo [a, b, *], Pedro Curto-Risso [a], Waldir Antonio Bizzo [b]

[a] Institute of Mechanical Engineering and Industrial Production, Faculty of Engineering, Universidad de la República, 11300 Montevideo, Uruguay
[b] Faculty of Mechanical Engineering, University of Campinas - UNICAMP, 13083-970 Campinas, SP, Brazil

ARTICLE INFO

Article history:
Received 16 October 2015
Received in revised form
27 January 2017
Accepted 30 January 2017

Keywords:
Biomass combustion
Numerical simulation
Biomass boilers
Sugarcane bagasse

ABSTRACT

A simple numerical model is presented to simulate the combustion of a biomass particle in a vertical stream. Emphasis focuses on the trajectories of spherical and cylindrical particles in the furnace. Combustion is modeled in three sequential stages: drying, pyrolysis and char combustion. Biomass consumption is determined by correlations based on Arrhenius kinetics and mass transfer parameters. Pyrolysis is modeled using five first-order kinetic equations considering the following products: volatiles, char and tar. The char consumption rate is modeled by three first-order kinetic equations, considering that char reacts with oxygen, carbon dioxide and water. The model is validated by comparing the duration of each simulated stage against experimental data taken from the literature. It is validated for spherical particles of up to 5 mm in diameter using a shrinking core model and for cylindrical particles of up to 3 mm using an ash-segregated model. Particle trajectory results are presented in order to determine the geometry and functional parameters of the combustion chamber that ensure complete suspension-firing. The combustion chamber geometry and biomass distributor height are determined as a function of airflow velocity and biomass characteristics for the combustion of bagasse with moisture contents of 30%–50% and particle diameters of 0.5 mm–3.5 mm. This study also allows the airflow velocity to be determined based on the boiler dimensions and the biomass characteristics to ensure that no particle ends up on the grate. After establishing the velocity, it is possible to determine what particle size will reach the top of the chamber or burn completely in suspension.

© 2017 Elsevier Ltd. All rights reserved.

Contents

* Corresponding author. Institute of Mechanical Engineering and Industrial Production, Faculty of Engineering, Universidad de la República, 11300 Montevideo, Uruguay.
E-mail address: germannace@gmail.com (G. Navarrete Cereijo).

http://dx.doi.org/10.1016/j.biombioe.2017.01.030
0961-9534/© 2017 Elsevier Ltd. All rights reserved.

Nomenclature

A_p	Particle projected area, m^2
A_s	Particle surface area, m^2
c_p	Specific heat at constant pressure, $J\ kg^{-1}K^{-1}$
C_D	Drag coefficient
d_p	Particle diameter, m
D	Mass diffusivity, m^2s^{-1}
E_a	Activation energy, $J\ mol^{-1}$
F_E	Buoyancy force, N
F_D	Drag force, N
$f_{p,i}$	View factor particle-surface i
G	Gravitational acceleration, $m\ s^{-2}$
H	Sensible specific enthalpy specie i, $J\ kg^{-1}$
h^l	Latent specific enthalpy, $J\ kg^{-1}$
h_j^q	Chemical specific enthalpy reaction j, $J\ kg^{-1}$
$\overline{h}$	Coefficient of thermal convection, $W\ m^{-2}K^{-1}$
$\overline{h}_m$	Coefficient of mass convection, $m\ s^{-1}$
k_c	Conductivity $W\ m^{-1}K^{-1}$
K	Kinetic coefficient
k_0	Arrhenius' Frequency factor
L_p	Particle length, m
M	Molecular mass, $kg\ mol^{-1}$
M	Mass, kg
m_0	Initial mass, kg
$\dot{m}$	Mass rate, $kg\ s^{-1}$
N	Reactant stoichiometric ratio
Nu_d	Nusselt's number based on particle diameter
Pr	Prandtl's number based on particle diameter
Pe_d	Péclet's number based on particle diameter
r_p	Particle radio, m
R	Universal gas constant, $J\ mol^{-1}K^{-1}$
Re_d	Reynolds' number
Sh_d	Sherwood's number
Sc	Schmidt's number
T	Absolute temperature, K
T_{ref}	Reference temperature, K
U_m	Global coefficient of mass transport, $m\ s^{-1}$
v	Velocity, $m\ s^{-1}$
Y_C	Initial fixed carbon in mass fraction
X	Molar fraction

Greek letters

α	Absorbance
ε	Porosity
λ	Air fuel equivalence ratio
μ	Dynamic viscosity, $kg\ m^{-1}s^{-1}$
ν	Cinematic viscosity, m^2s^{-1}
ρ	Density, $kg\ m^{-3}$
σ	Stefan-Boltzmann constant, $W\ m^{-2}K^{-4}$
τ	Tortuosity

Subscripts

c	Char
b	biomass
g	Furnace environment gas
H_2O	Water
mix	Gas mixture
p	Particle
s	Surface
sp	Surrounding particles
tar	Tar
vol	Volatiles
i	specie i
j	reaction j

1. Introduction

The design of industrial boilers requires optimum understanding of the different phenomena that occur during the combustion of a biomass particle. Such knowledge contributes to improve constructive and functional parameters pertaining to biomass feed, air injection and combustion itself. In the earliest bagasse boiler models, the main combustion took place on the grate and involved large amounts of unburned residues that had to be removed from the boiler. Since then, biomass combustion systems have evolved continually to achieve suspension-firing of biomass, with a smaller fraction of grate-firing. This is possible because of secondary air injection heating, as shown in Fig. 1 [1]. The vast majority of bagasse boilers employed in Brazils sugar and alcohol industry use intermittently moving grates or water cooled pinhole grates. The bagasse is fed into the furnace mechanically or by gravity and the distribution of bagasse in the chamber is usually improved by means of air jets. The smaller particles are dragged by the gases and the combustion process takes place in suspension. However, larger particles settle onto the grate and the combustion process takes place in a fixed bed regime [2].

Particle combustion begins when the bagasse comes into contact with the hot gases, and involves three main stages: drying, devolatilization and char combustion. In general, the devolatilization stage is modeled as pyrolysis. The stages can be simultaneous or sequential, depending on particle size and shape [3]. Most studies have used simultaneous-stage models in which drying and oxidation occur in infinitesimal layers, while pyrolysis takes place in a finite volume considering local thermal equilibrium. In those models, the biomass is divided into four different zones: unreacted wet biomass, pyrolytic zone, unburned char, and ashen zone [4,5]. Other models consider that the last two stages may be

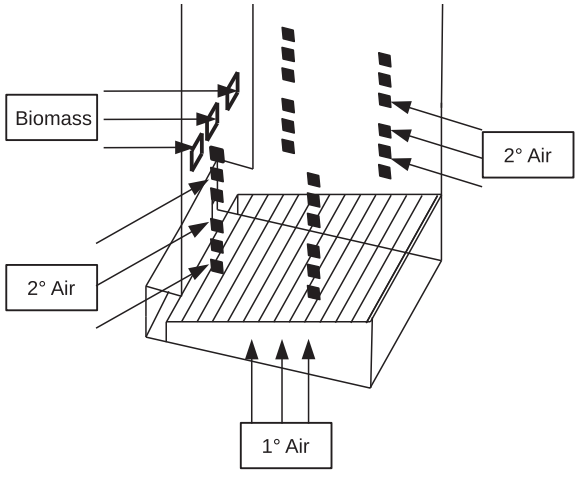

Fig. 1. Bagasse boiler - functional diagram.

simultaneous or sequential, depending on the oxygen concentration at the particle surface [6]. In the pyrolytic stage, the combustion of the volatiles can reduce the amount of oxygen at the particle surface to zero. Consequently, the combustion of volatiles takes place away from the particle and the combustion of char cannot occur [7].

Some authors model the drying process based on mass transport due to the differences in partial pressure, in which the particle temperature is determined by heat transfer [3,8]. Other authors model the drying process based on a drying front, which is determined by the temperature and enthalpy of evaporation [4,5].

Thermochemical processes such as pyrolysis, gasification and combustion involve numerous combined phenomena such as homogeneous and heterogeneous chemical reactions, heat transfer, mass and momentum transport [9,10]. The reactions between two stable chemical species are a complex combination of many elementary reactions. The sequence of these reactions is defined as chain reaction mechanisms that are constituted by many series and parallel reactions [10,11]. In many types of reactions, the reaction rate α, related to mass change or reagent volume, can be determined as a function of Arrhenius parameters (k_0, E_a), absolute temperature (T) and composition.

Pyrolysis is the most complex stage. Its kinetics can be modeled from a single global equation to complex models with hundreds of parallel and series equations representing complex reaction mechanisms. Some authors consider that biomass undergoes primary decomposition into volatiles, tar and char, and secondary decomposition of tar into volatiles and char [3,12]. Other authors consider a similar process in which the biomass decomposes into noncondensable gases, condensable gases and char [4,6,8]. The main noncondensable gases are CO, CO_2, CH_4 and H_2. The condensable gases can be represented by their elemental composition $C_xH_yO_z$ [6]. Furthermore, secondary decomposition of condensable gases into noncondensable gases can be considered [13]. Biomass pyrolysis can also be modeled by the parallel decomposition of its main components: lignin, cellulose, hemicellulose and extractives [5,14].

More complex models consider the decomposition in a larger number of species. These models are defined as Structural Models and an example of this is the Functional Groups model. This model considers decomposition into the following components: nonvolatilizable carbon, hydrogen abstraction by tar, light volatiles (CO_2, CO, H_2O), light and heavy hydrocarbons (CH_4, C_2H_4, C_2H_6, C_3H_6, C_3H_8), and hydrogen (H_2). Here, the consumption and formation of the different components are determined from a first order kinetic equation based on the Arrhenius parameters, temperature and composition [15–17].

The majority of studies model char combustion as direct combustion with O_2 and gasification with H_2O and CO_2 as reactants. The reaction kinetics depends on the Arrhenius parameters, temperature, pressure, and on the concentration of reactants [3,5,18]. At this point, it is necessary to define the model for ash behavior. Two cases are considered in this paper: the shrinking-core model [3–5] and the ash-segregated model [7,19]. In the first model, the ashes adhere to the surface, forming a layer that hinders heat and mass transfer. The second model considers that the ashes are in the form of small loose particles that are detached from the particle. Therefore, the core is always exposed to environmental gases [10].

Some experimental works describe the evolution of biomass particle combustion based on images captured with a high-speed camera [20–22], and use those images to validate the model of both spherical and cylindrical particles.

The aim of this work is to develop a simple numerical model to simulate the combustion of biomass particles and their trajectory in order to determine the vertical dimensions of the combustion chamber that will ensure suspension-firing. The main stages are considered to be sequential. For the drying and char combustions stages, the particle is selected as a single control volume. Devolatilization is modeled as pyrolysis by discretizing the particle into small volumes. The trajectory of the particle is also modeled in a one-dimensional scheme in order to analyze its flight path in an air flow when it burns. Based on these results, the combustion chamber geometry and biomass distributor height are determined as a function of airflow velocity and biomass characteristics. This study also allows the airflow velocity to be determined based on the boiler dimensions and the biomass characteristics to ensure that no particle ends up on the grate. After establishing the velocity, it is possible to determine what particle size will reach the top of the chamber or burn completely in suspension.

2. Mathematical model of a single particle

In this paper, the combustion of a single particle suspended in a one-dimensional flow is modeled considering both cylindrical and spherical cases. The model is developed in three sequential steps: 1) drying, 2) pyrolysis and volatile combustion, and 3) char gasification and char combustion. The drying step is determined by energy balance assuming an evaporation temperature of 100 °C at the particle surface. Pyrolysis is modeled by five first-order kinetic equations based on Arrhenius parameters representing volatiles, char and tar formation, and tar decomposition in volatiles and char. The volatiles represent noncondensable gases while the tar represents condensable gases. Char combustion is modeled by three first-order global kinetic equations based on Arrhenius parameters that represent direct char oxidation and char gasification with H_2O and CO_2, differentiating between ash-segregated diffusion and shrinking-core models.

2.1. Energy balance

Kinetic reactions are strongly dependent on the particle's temperature; hence, before analyzing each stage, we describe the general energy balance applied to the particle in equation (1). It is assumed that work is zero, heat transfer occurs by convection and radiation, and pressure on the particle is constant and equal to chamber pressure.

$$m_p\, c_p\, \frac{dT_p}{dt} + \frac{dm_p}{dt}\, c_p \left(T_p - T_{ref}\right) = A\,\sigma\Big[\sum f_{p,i}\,\varepsilon_p\left(T_i^4 - T_p^4\right) + \left(\varepsilon_g T_g^4 - \alpha_g T_p^4\right)\Big] + A\,\overline{h}\left(T_g - T_p\right) - \dot{m}_{H_2O} h_{fg} + \sum_i \dot{m}_i h + \sum_j \dot{m}_j \Delta h_j^q \tag{1}$$

The first term at the right represents heat transfer by radiation to surrounding surfaces and gases. The second term represents heat transfer by convection. The third term represents the latent energy, while the fourth represents the energy leaving the control volume by mass flux through the boundaries, and the last term represents the chemical energy released by each reaction j. The emissivity, ε_g, and absorptivity of the gases, α_g, are determined by the correlations presented by Leckner et al. [23], based on Hottels method. Heat transfer by convection is modeled by the correlations presented in Bejan and Kraus [24], equation (2) for spheres, equation (3) ($Pe_d > 0,2$) and equation (4) ($Pe_d < 0,2$) for cylinder shapes.

$$\frac{\overline{h}\, d_p}{k_c} = 2 + \left(0,4\, Re_d^{1/2} + 0,06\, Re_d^{2/3}\right) Pr^{0,4} \left(\frac{\mu_\infty}{\mu_w}\right)^{1/4} \quad (2)$$

$$\frac{\overline{h}\, d_p}{k_c} = 0,3 + \frac{0,62\, Re_d^{1/2} Pr^{1/3}}{\left[1 + (0,4/Pr)^{2/3}\right]^{1/4}} \left[1 + \left(\frac{Re_d}{282.000}\right)^{5/8}\right]^{4/5} \quad (3)$$

$$\frac{\overline{h}\, d_p}{k_c} = \frac{1}{0,8237 - 0,5 \ln(Pe_D)} \quad (4)$$

2.2. Drying

The drying rate is determined based on the energy balance, assuming a particle evaporation temperature of 100 °C, as presented in equation (5).

$$\dot{m}_{H_2O} \frac{h_{fg}}{A_p} = \sigma\left[\varepsilon_p\left(T_w^4 - T_p^4\right) + \left(\varepsilon_g T_g^4 - \alpha_g T_p^4\right)\right] + \overline{h}(T_g - T_p) \quad (5)$$

In this stage, an unexposed core model is considered in which the heat and mass transfer rates are relatively rapid, determining a homogeneous intraparticle temperature and instantaneous species diffusion.

2.3. Pyrolysis

Devolatilization is modeled as fast pyrolysis, based on five global reactions presented in Table 1, whose respective mass reaction rates are presented in equations (6)–(9). These reactions correspond to the biomass consumption rate, tar formation and decomposition rates, and char and volatile formation rates. This stage requires working with a one-dimensional finite volume approach inside the particle because it improves the results considerably. Equation (10) represents the kinetic coefficient k as a function of the Arrhenius parameters k_0 and E_a for each reaction.

$$\frac{dm_b}{dt} = -(k_1 + k_2 + k_3)\, m_b \quad (6)$$

$$\frac{dm_{tar}}{dt} = k_2\, m_b - (k_5 + k_4)\, m_{tar} \quad (7)$$

$$\frac{dm_c}{dt} = k_3\, m_b + k_5\, m_{tar} \quad (8)$$

$$\frac{dm_{vol}}{dt} = k_1\, m_b + k_4\, m_{tar} \quad (9)$$

$$k_j = k_{0j}\, exp\left(-\frac{E_{a_j}}{R\,T}\right) \quad (10)$$

Table 1
Kinetic parameters of pyrolysis.

Index	Reaction	$E_{a_j}(kJ\ mol^{-1})$	$k_{0j}(s^{-1})$	Ref.
1	biomass→volatiles	177.0	1.11×10^{11}	[25]
2	biomass→tar	149.0	9.28×10^{9}	[25]
3	biomass→char	125.0	3.05×10^{7}	[25]
4	tar→volatiles	107.5	4.28×10^{6}	[26]
5	tar→char	107.5	1.00×10^{6}	[3,12]

The combustion of volatiles is modeled as a sheet of flame with one infinitely fast global reaction in the stoichiometric ratio [18]. Hence, the concentration of oxygen and volatile fuel in the flame are considered zero. The flame front is modeled as a sphere in spherical particles and as a cylinder without ends in cylindrical particles. Equation (11) represents the general stoichiometric equation of pyrolysis including the combustion of volatiles. This equation is only used to determine the composition of volatiles that leave the control volume. It is considered that the tar reacts completely, turning into char and volatiles. With regard to energy balance, an intermediate amount of tar is considered at each instant, depending on the kinetic equations. The volatiles are modeled based on the expression $C_{a/12}\, H_b\, O_{c/16}\, N_{d/14}$, in which a, b, c and d represent the amount of each element considering the same elemental composition of the biomass without the amount of fixed carbon. This hypothesis is used to simplify the model, because otherwise one kinetic equation would be needed for each product, expanding the system into dozens of equations.

$$C_{\frac{a}{12}} H_b O_{\frac{c}{16}} N_{\frac{d}{14}} + \left[\frac{a}{12} + \frac{b}{4} - \frac{c}{32}\right](O_2 + 3,76 N_2) \rightarrow \frac{a}{12}\, CO_2 + \frac{b}{2}\, H_2O + \left\{3.76\left[\frac{a}{12} + \frac{b}{4} - \frac{c}{32}\right] + \frac{d}{28}\right\} N_2 \quad (11)$$

$$\dot{m}_{O_2} = -\left[\frac{a}{12} + \frac{b}{4} - \frac{c}{32}\right] M_{O_2}\, \frac{dm_{vol}}{dt} \quad (12)$$

$$\dot{m}_{CO_2} = \frac{a}{12}\, M_{CO_2}\, \frac{dm_{vol}}{dt} \quad (13)$$

$$\dot{m}_{H_2O} = \frac{b}{2}\, M_{H_2O}\, \frac{dm_{vol}}{dt} \quad (14)$$

The reaction and species transfer rates determine the location of the volatile flame: at the surface or away from it. After determining the mass flow rates from equation (9) and equations (12)–(14), it is necessary to determine where the flame occurs. It will be within the radius in which the mass flow of oxygen carried by convection equals the amount of oxygen required for the combustion of the volatiles. If this radius is smaller than the particle radius, the combustion occurs at the surface; otherwise, it occurs within the given radius. Equation (15) gives the mass of oxygen transferred by convection from a remote distance to the flame.

$$\dot{m}_{O_2} = A\, \overline{h}_m\, (X_{\infty_{O2}} - X_{ch_{O2}})\rho_{mix}\, \frac{M_{O_2}}{M_{mix}} \quad (15)$$

The convection mass transport coefficient is determined by equation (16) ($3,5 < Re_d < 7,6 \times 10^4$) for spherical particles, and by equation (17) ($Re_d\, Sc > 0,2$) and equation (18) ($Re_d\, Sc < 0,2$) for cylindrical particles [24].

$$\frac{\overline{h_m}\, d_p}{D} = 2 + \left(0,4\, Re_d^{1/2} + 0,06\, Re_d^{2/3}\right) Sc^{0,4} \quad (16)$$

$$\frac{\overline{h_m}\, d_p}{D} = 0,3 + \frac{0,62\, Re_d^{1/2} Sc^{1/3}}{\left[1 + (0,4/Sc)^{2/3}\right]^{1/4}} \left[1 + \left(\frac{Re_d}{282.000}\right)^{5/8}\right]^{4/5} \quad (17)$$

$$\frac{\overline{h_m}\, d_p}{D} = \frac{1}{0,8237 - 0,5 \ln(Re_d\, Sc)} \quad (18)$$

Particle temperature is determined by calculating an energy balance for each control volume. The chemical energy of the pyrolysis reaction, including the five reactions listed in Table 1, are determined by equation (19), which is valid for an initial fixed carbon content of less than 27% [27]. Each balance includes the sensible energy of the biomass, tar, and volatiles.

$$\Delta h^q = -1460\, Y_C + 538\,(1 - Y_C) \tag{19}$$

2.4. Char combustion

The char combustion stage is modeled as a direct combustion with O_2 and parallel gasification with CO_2 and H_2O as reactants. The kinetic equations for each reaction are modeled by equation (20), based on the Arrhenius law. This equation models the mass flow of carbon being consumed as a function of the absolute particle temperature and reactant mole fraction at the surface. The Arrhenius parameters for each equation are presented in Table 2.

$$\dot{m}_{C,j} = A_s k_{0i}\, exp\left(-\frac{E_{ai}}{RT_s}\right) \frac{M_C}{n_i} \frac{p}{R\,T_s} X_{i,s} \tag{20}$$

The mole fractions at the surface are determined by the species mass balance (equations (21)–(23)) and mass transport. To simplify the model, it is considered that the carbon monoxide and molecular hydrogen produced during gasification are burned far away from the particle.

$$\dot{m}_{O_2} = -\frac{M_{O_2}}{M_C}\, n_{O_2}\, \dot{m}_{C,6} \tag{21}$$

$$\dot{m}_{CO_2} = \frac{M_{CO_2}}{M_C}\,(\dot{m}_{C,6} - \dot{m}_{C,7}) n_{CO_2} \tag{22}$$

$$\dot{m}_{CO} = n_{CO}\, \frac{M_{CO}}{M_C}\, (2\,\dot{m}_{C,7} + m_{C,8}) \tag{23}$$

$$\dot{m}_{H_2O} = -n_{H_2O}\, \frac{M_{H_2O}}{M_C}\, \dot{m}_{C,8} \tag{24}$$

The transport of each species is modeled by mass convection away from the particle and diffusion through the inert layer by equation (25).

$$\dot{m}_i = A_s\, U_m\, (X_{i,s} - X_{i,\infty})\rho\, \frac{M_i}{M_{mix}} \tag{25}$$

X_{is} and $X_{i\infty}$ are the molar fractions of each species at the particle surface and in the reservoir, respectively. U_m represents the global mass transfer coefficient determined by equations (26) and (27) for spherical and cylindrical shapes, respectively.

$$\frac{1}{U_m} = \frac{r_2^2}{D_m}\left(\frac{1}{r_1} - \frac{1}{r_2}\right) + \frac{1}{h_m} \tag{26}$$

$$\frac{1}{U_m} = \frac{r_2}{r_1\,\bar{h}_m} + \frac{r_2}{D_m} \ln(r_2/r_1) \tag{27}$$

The convective mass transfer coefficient $\bar{h}_m$ is determined from equations (16)–(18), depending on the flow conditions and particle shape. Intraparticle diffusivity is determined by equation (28) as a function of particle porosity and tortuosity. Tortuosity is defined as the ratio of the effective length of the flow path to the length in the porous sample [30]. This parameter is taken into account in the shrinking core model, and according to de Souza-Santos [10], tortuosity can be approximated as the inverse of porosity. In the ash-segregated model, the global mass transfer coefficient U_m is modeled by the convective mass transfer coefficient $\bar{h}_m$. In equation (28), diffusion is presented as a function of the selected ash model.

$$D_m = \frac{\varepsilon\, D_g}{\tau} \tag{28}$$

$$D_m = \begin{cases} \infty & \text{ash} - \text{segregated model} \\ \varepsilon^2\, D_{gas} & \text{shrinking core model} \end{cases} \tag{29}$$

By solving the equation system, the mass of char being burned can be calculated directly as a function of known parameters, using equations (30)–(32). The term outside the parenthesis represents the mass transfer coefficient including diffusion, convection and kinetic parameters. The term inside the parenthesis represents the number of species *i* that come from outside the particle. In equation (31), a second term must be included to represent the CO_2 formed in reaction 6.

$$\dot{m}_{C,6} = \frac{k_6\, U_m}{k_6 + U_m}\left[A_s \frac{M_C}{n_{O_2}} \frac{p}{RT_s}\, X_{O_{2\infty}}\right] \tag{30}$$

$$\dot{m}_{C,7} = \frac{k_7\, U_m}{k_7 + U_m}\left[A_s \frac{M_C}{n_{CO_2}} \frac{p}{RT_s}\, X_{CO_{2\infty}} + \frac{\dot{m}_{C,6}}{U_m}\right] \tag{31}$$

$$\dot{m}_{C,8} = \frac{k_8\, U_m}{k_8 + U_m}\left[A_s\, \frac{M_C}{n_{H_2O}}\, \frac{p}{R\,T_s} X_{H_2O_\infty}\right] \tag{32}$$

The particle temperature is considered homogeneous and is determined by solving the energy balance presented in equation (1). The energies of the chemical reactions are determined from the formation enthalpies, considering carbon as a pure substance [31]. The specific enthalpy of each chemical reaction is described in Table 3.

2.5. One-dimensional particle trajectory

The particle trajectory is determined by the balance of forces applied to the particle, as illustrated in Fig. 2. The forces considered here are weight, drag, F_D, and buoyancy, F_E.

$$m_p\, \frac{dv_p}{dt} + (v_h - v_p)\, \frac{d\dot{m}_p}{dt} = F_E + F_D - m_p\, g \tag{33}$$

Assuming that the burned gas velocity, v_h, is equal to the particle velocity, v_p, the expressions of forces are substituted as follows:

Table 2
Kinetic parameters of char reactions.

Index	Reaction	$E_{a_j}(kJ\ mol^{-1})$	$k_{0j}(m\ s^{-1})$	Ref.
6	$C + O_2 \rightarrow CO_2$	68.0	4.65×10^4	[28]
7	$C + CO_2 \rightarrow 2CO$	138.0	7.37×10^3	[29]
8	$C + H_2O \rightarrow CO + H_2$	138.0	7.37×10^3	[29]

Table 3
Char reactions and chemical energies at 25 °C.

Index	Reaction	$\Delta h^q_{C,j}(kJ\ kg^{-1})$
6	$C + O_2 \rightarrow CO_2$	32 814.7
7	$C + CO_2 \rightarrow 2CO$	−14 381.8
8	$C + H_2O \rightarrow CO + H_2$	−10 949.3

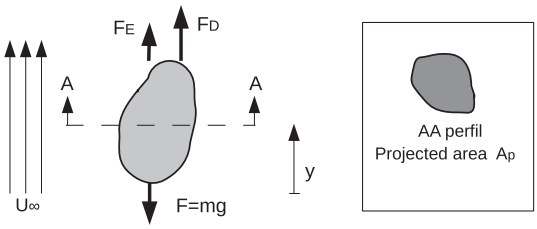

Fig. 2. Forces diagram applied to the particle [32].

$$m_p \frac{dv_p}{dt} = V_p\, g\left(\rho_g - \rho_p\right) + \frac{1}{2}\rho_f \left(v_g - v_p\right)^2 A_p\, C_D \tag{34}$$

The drag coefficient, C_D, is modeled by equation (35) for $Re_p < 2,6 \times 10^5$. The parameters A, B, C, D depend on the particle sphericity, ϕ [33].

$$C_D = \frac{24}{Re_p}\left(1 + A\, Re_p^B\right) + \frac{C}{1 + \frac{D}{Re_p}} \tag{35}$$

To apply this balance requires knowledge about some of the dimensional characteristics of the particle, such as length, L_p, projected area, A_p, and density, ρ_p, as a function of particle diameter, d_p. Table 4 and equations (36)–(38) present results and correlations for these characteristics, based on the result obtained by Lenço [32] for a typical sugarcane bagasse particle size distribution.

$$L_p = 3,827\, d_p - 0,414 \times 10^{-3} \tag{36}$$

$$A_p = -105,9 \times 10^3 d_p^4 + 480,2\, d_p^3 + 1,6246 d_p^2 + + 0,9941 \times 10^{-3} d_p - 0,2173 \times 10^{-6} \tag{37}$$

$$\rho_p = -21,135\,(1000\, d_p)^3 + 205,37\,(1000\, d_p)^2 + -556,59\,(1000\, d_p) + 632,09 \tag{38}$$

2.6. Validation

A simple and fast Fortran routine, BPSC-Sim, was developed to study the combustion of a single biomass particle [34]. The model was validated comparing the prediction times for each stage with experimental data taken from the literature, considering spherical and cylindrical particles.

For spherical particles, the combustion times of each stage obtained by the model were compared with the experimental results presented by Mason et al. [22] for eucalyptus, pine and willow. The characterization of these biomass and the experimental conditions are described in Table 5. As can be seen in Fig. 3, the model was validated for particles with a diameter of up to 5 mm for the three biomasses, and the best fit was obtained by using the shrinking core model.

The combustion times for cylindrical particles were validated by comparing them with the experimental results presented by Momeni et al. [21]. Table 6 describes the characterization of the biomasses and the experimental conditions. As Fig. 4 shows, the ash-segregated model presented better results for cylindrical particles, and was validated reasonably well for particles with a diameter of up to 3 mm and a length of up to 18 mm.

With regard to surface temperature and mass consumption, it is difficult to obtain experimental results at high heating rates and with small particles because the combustion process is so fast. However, some results for mass evolution as a function of time have shown that the slope of each stage of combustion can be considered constant [2,3,6,19]. In Fig. 5, the evolution of specific mass (measured) and temperature (simulated) for 0.24 mm straw particles reported by Saastamoinen et al. [19] is compared with the present model, where the specific mass is the rate of mass and initial mass of the particle. The simulation was made based on the characterization of biomasses and experimental conditions described in Table 7. The mass evolution fits well with the experimental; however, the evolution of surface temperature shows a different behavior, mainly in the pyrolysis stage and in the transition to the char combustion stage. The maximum temperature is similar and corresponds to the char combustion stage. The difference in the temperature of the pyrolysis stage was attributed to the sequential stages of the model. In the real process, the outer layers of char begin to burn before the end of the pyrolysis stage, so the surface is the first part that is pyrolyzed, immediately leading to char combustion, causing high temperatures at the surface. To take this behavior into account one must consider simultaneous processes inside the particle.

In summary, the evolution of time and mass of spherical particles with diameters of up to 5 mm was validated using the shrinking core model and that of cylindrical particles of up to 3 mm using the ash-segregated model.

Table 4
Dimensional characterization of bagasse. Moisture content: 7.5% wet basis [32].

Mass fraction	$A_p(mm^2)$	$L_p(mm)$	$d_p(mm)$	$\rho_p(kg\ m^{-3})$
14.8%	0.19	0.54	0.28	503.04
9.90%	2.27	2.57	0.90	259.57
17.7%	7.65	6.18	1.75	185.02
21.3%	8.77	6.96	1.78	217.81
10.9%	21.46	11.66	2.98	225.82
6.10%	33.81	14.46	4.05	239.55
19.3%	59.48	17.21	4.09	429.15

3. Results

This section presents the evolution of mass and temperature of the bagasse combustion process and the study of particle velocity and trajectory. The conditions of the simulation are described in

Table 5
Characterization of biomass and experimental conditions.

Parameters	Basis	Eucalyptus	Pine	Willow
Ultimate analysis (mass fraction)				
C	daf	49.2%	47.4%	50.8%
H	daf	5.6%	5.3%	6.0%
O	daf	45.1%	45.9%	42.7%
N	daf	0.1%	1.3%	0.4%
Proximate analysis (mass fraction)				
Volatile content	daf	82.5%	82.5%	83.6%
Fixed carbon	daf	17.5%	17.5%	16.4%
Ash	dry	0.9%	2.0%	1.9%
Other characteristics				
Density ($kg\ m^{-3}$)	dry	670	480	520
GCV($MJ\ kg^{-}1$)	dry	19.4	18.6	19.8
Parameters		**Symbol**	**Value**	**Unit**
View factor particle-walls		$f_{p,w}$	1	–
Walls temperature		T_w	1173	K
Gas temperature		T_g	1823	K
Air fuel equivalence ratio		λ	2.5	–

Source: Mason et al. et al. [22].

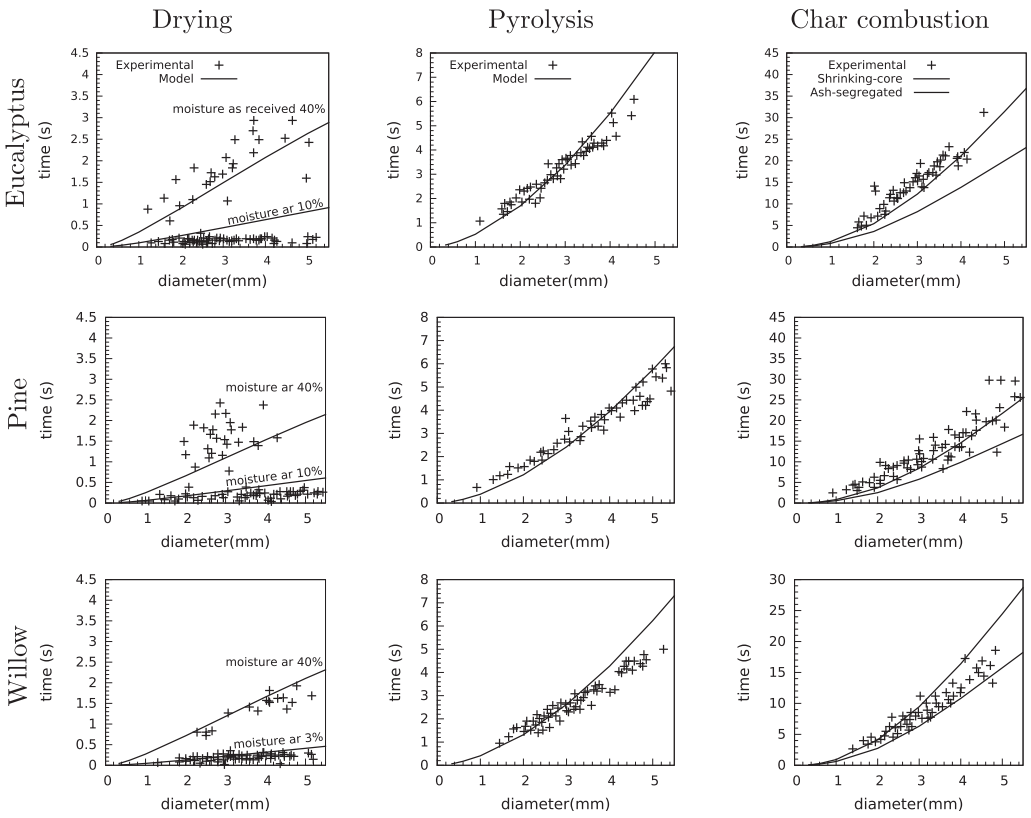

Fig. 3. Model duration of the different stages compared with experimental data for spherical particles from Mason et al. [22]. ar: as received basis.

Table 6
Characterization of biomass and experimental conditions.

Parameter	Value	Basis
Ultimate analysis (mass fraction)		
C	45.8%	daf
H	5.95%	daf
O	47.9%	daf
N	0.4%	daf
Proximate analysis (mass fraction)		
Volatile content	85.6%	daf
Fixed carbon	14.4%	daf
Ash	0.3%	dry
Other characteristics		
Density ($kg\ m^{-3}$)	600	dry
GCV($MJ\ kg^{-1}$)	16.98	dry
Parameter	**Value**	**Unit**
View factor particle-walls	1	–
Walls temperature	1473	K
Gas temperature	1673	K
Air fuel equivalence ratio	1.36	–

Source: Momeni et al. [21].

Tables 8 and 9. The only interaction with other particles is considered to occur through heat transfer by radiation.

Fig. 6 illustrates the evolution of temperature and specific mass of spherical and cylindrical (bagasse) particles using the ash shrinking core and ash-segregated models, respectively. The three main stages were determined based on the changes in the slope of the mass evolution curve and the breaks in the temperature curve. Note the initial heating ramp up to the drying temperature, followed by a constant temperature during this stage, and then another heating ramp without any reaction up to the pyrolysis temperature. Pyrolysis begins within the range of 800–900 K and ends at 1200 K. These high temperatures are a consequence of the high heating determined by the neighboring conditions. Finally, note the onset of char combustion, which is characterized by a rapid rise in temperature until it stabilizes. The amount of residual char after pyrolysis should be less than that remaining in the proximate analysis, in which the conditions are optimal to obtain a high amount of carbon.

To analyze the particle trajectory and velocity, results are presented based on variations in particle shape and size, air velocity and moisture. The other functional parameters are kept fixed, as listed in Table 8.

Fig. 7 depicts particle trajectory and velocity curves for different particle sizes and shapes. Smaller particles tend to be dragged during the entire combustion process, while larger ones tend to settle during the initial stages. When the forces of drag and buoyancy are greater than the weight as a result of the consumption of mass without change in the particle size, the particles begin to be dragged.

The difference between the greatest and smallest heights reached by the particle must be taken into account in order to determine the geometry of the chamber. The location of the biomass distributor is determined based on the absolute value of the minimum height. Fig. 8 presents these limits as a function of the airflow velocity, size and moisture content of cylindrical particles. This figure shows the dimensions based on only one particle size, so they are not representative of the whole group of bagasse particle shapes and sizes.

To determine the chambers dimensions for a set of diameters, the maximum (> 0) and minimum (< 0) height that the group of particles can reach at each air velocity must be considered. The absolute value of the minimum height determines the distributor height and the difference between the maximum and the

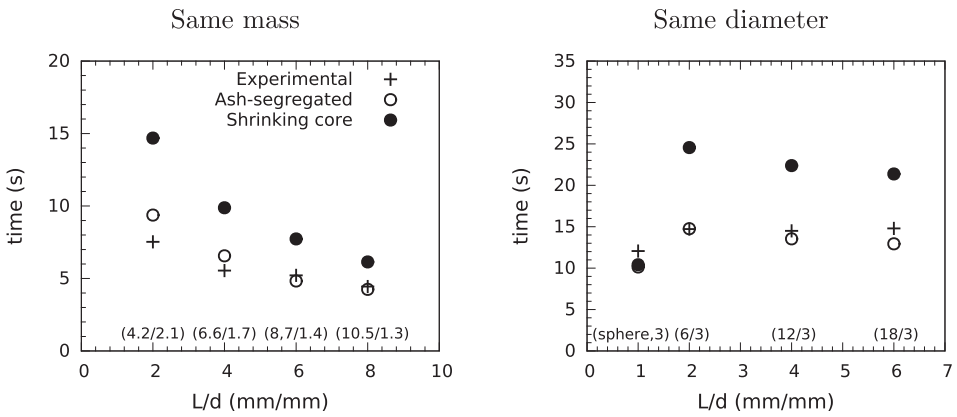

Fig. 4. Cylindrical particles compared with experimental results from Momeni et al. [21].

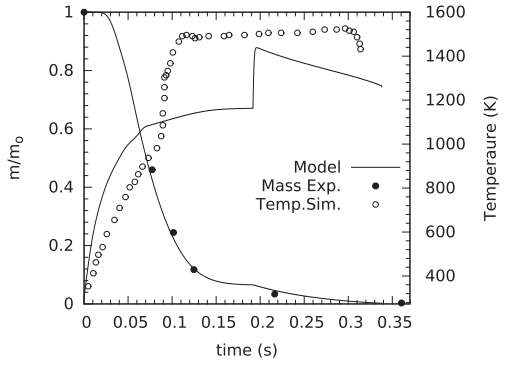

Fig. 5. Model mass evolution compared with experimental result and model temperature evolution compared with simulation results from Saastamoinen et al. [19].

Table 7
Characterization of biomass and experimental conditions.

Parameter	Value	Basis
Ultimate analysis (mass fraction)		
C	44.0%	daf
H	5.5%	daf
O	50.17%	daf
N	0.33%	daf
Proximate analysis (mass fraction)		
Volatile content	83.2%	daf
Fixed carbon	16.8%	daf
Ash	0.5%	dry
Other characteristics		
Density ($kg\ m^{-3}$)	500	dry
GCV($MJ\ kg^{-1}$)	19.78	dry
Parameter	**Value**	**Unit**
View factor particle-walls	1	–
Walls temperature	1123	K
Gas temperature	1173	K
Air fuel equivalence ratio	1.36	–

Source: Saastamoinen et al. [19].

minimum height determines the chamber height. Both heights are presented in Fig. 9 for groups of particles ranging in diameter from 0.5 to 2.5 mm, 0.5–3.0 mm, and 0.5–3.5 mm, and three different moisture contents.

The diagrams in Fig. 9 can also be used to determine the operating parameters for an existing boiler as a function of the furnace dimensions and biomass characteristics. The next paragraph offers an example of how to use the different diagrams.

Table 8
Fixed functional parameters.

Parameter	Symbol	Value	Unit
View factor particle-walls	$f_{p,w}$	0.2	–
Walls temperature	T_w	550	K
Surrounding particles mean temperature	T_{sp}	1173	K
View factor particle-surrounding particles	$f_{p,sp}$	0.8	–
Gas temperature	T_g	1173	K
Air fuel equivalence ratio	λ	1.4	–
Pressure	p	101300	Pa

Table 9
Characterization of biomass.

Parameter	Value	Basis	Ref.
Ultimate analysis (mass fraction)			
C	42.61%	daf	[35]
H	5.92%	daf	[35]
O	50.72%	daf	[35]
N	0.63%	daf	[35]
S	0.12%	daf	[35]
Proximate analysis (mass fraction)			
Volatile content	85.97%	daf	[36]
Fixed carbon	14.03%	daf	[36]
Ash	5.20%	dry	[36]
Other characteristics			
GCV($MJ\ kg^{-}1$)	17.72	dry	[35]
Porosity	0.4	–	estimated.

Consider a boiler with a furnace height of 40 m, a biomass distributor at a height of 20 m, burning bagasse with particle diameters of up to 3.5 mm and a moisture content of 50%. The height of the distributor was selected in order to explain the diagrams and to facilitate suspension-firing at low air flows and high biomass moisture content, according to Fig. 8b. If the goal is suspension combustion, airflow velocity should be the first parameter to be determined in order to ensure that no particle falls to a height of less than 20 m inside the furnace. To this end, the diagram (Fig. 9a) is marked with an H_d of 20 m and velocity is determined when it intersects the curve of 50% moisture content. In this case, airflow velocity is 4.35 m/s. After this, one must check whether the chamber is sufficiently tall to enable all the particles to burn before they reach the top. This is verified based on the air velocity and height of the chamber. If the point is above the H_T curve, all the particles are burned in suspension, and if it is not, some particles reach the top of the furnace. In this case, an H_T of 69 m is needed,

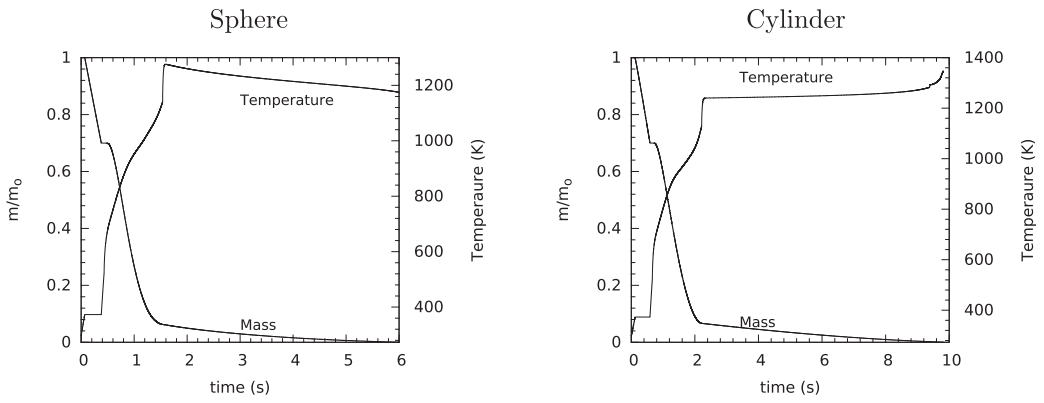

Fig. 6. Mass and temperature evolution for spherical and cylindrical particles with 2 mm of diameter and moisture of 30%.

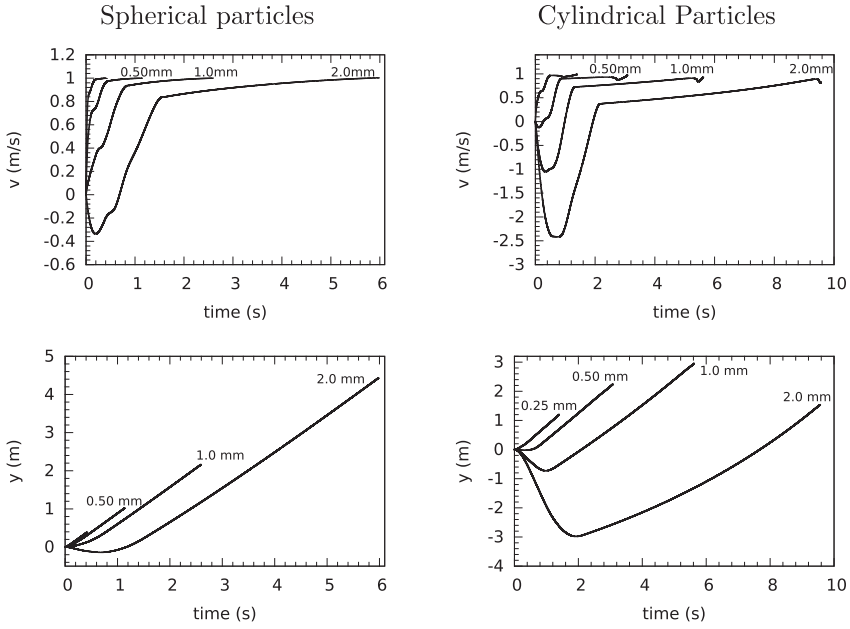

Fig. 7. Particle Velocity (v) and trajectory (y) for spherical and cylindrical shapes. Air flux velocity 1 m/s.

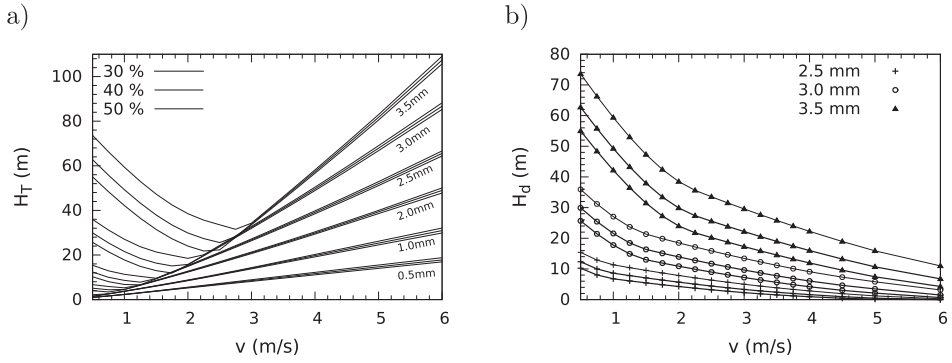

Fig. 8. a) Chamber height and b) bagasse distributor height in function of diameter and air velocity for moistures of 30%, 40% and 50% wet base.

but the boiler has an H_T of 40 m, so some particles reach the top. To determine which particles reach the top of the furnace, the diagram 9 d is used. This is determined based on the air velocity (v = 4.35 m/s) and the difference between the height of the furnace and that of the distributor ($H_T - H_d = 20$ m). The curves that lie above this point determine which diameters do not burn completely in suspension. In the case described here, particles with diameters larger than 1 *mm* do not burn completely before reaching the top.

Another point is to ensure the complete combustion of all the particles inside the furnace. Airflow velocity is determined from the

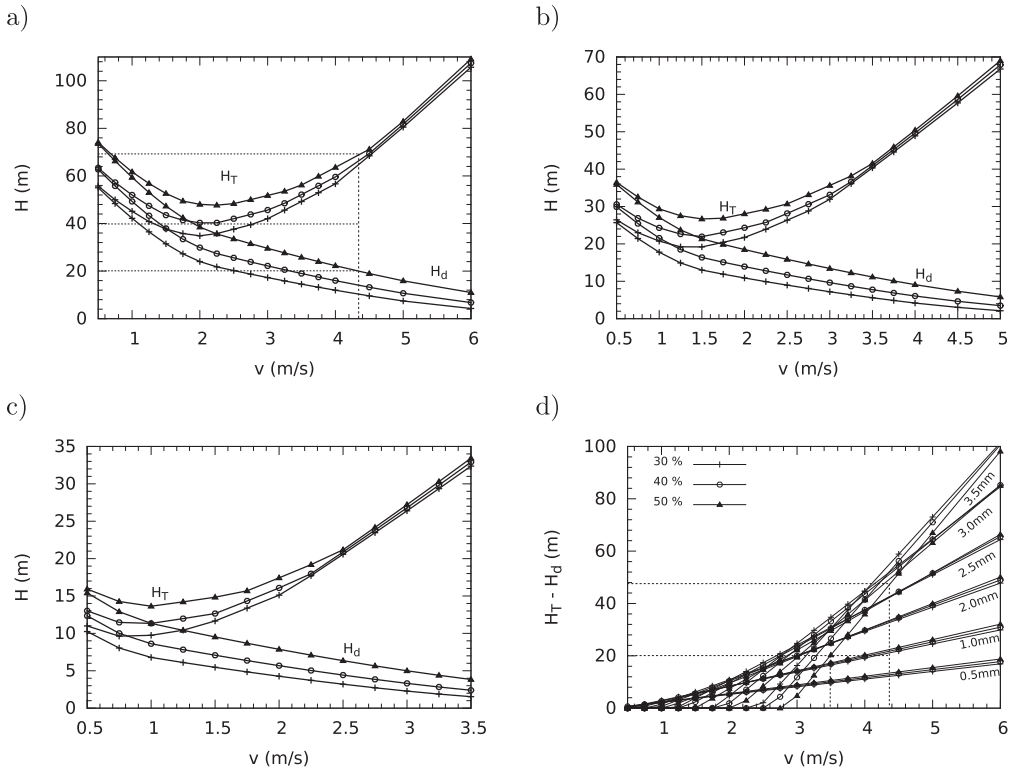

Fig. 9. Combustion chamber height and biomass distributor height for a group of particles between: a) 0.5–3.5 mm b) 0.5–3.0 mm c) 0.5–2.5 mm, in function of air velocity and for moistures of 30%, 40% and 50% wet base. d) Particle maximum height above the distributor in function of diameter and air velocity.

difference between the height of the furnace and that of the distributor ($H_T - H_d = 20$ m), using diagram 9 d. An airflow velocity of 3.45 m/s is determined. This ensures that all the particles burn completely in the furnace; however, some of them burn on the grate. An analysis of Fig. 8b indicates that particles larger than 3.2 mm burn partially on the grate.

This example shows that the best solution is not always to burn all the particles in suspension. The selection of the best configuration also involves analyzing the rate of heat transfer to water. In addition, a comparison of diagrams a, b and c in Fig. 9 indicates that suspension combustion and lower air velocities in smaller furnaces can be ensured by reducing the maximum particle diameter and moisture content.

4. Conclusions

A simple and fast Fortran routine was developed to study the combustion of a single biomass particle. The model was validated for spherical particles with diameters of up to 5 mm using the shrinking core model, and for cylindrical particles of up to 3 mm using the ash-segregated model.

This routine enables one to determine the evolution of particle mass, temperature and composition, in addition to other parameters. However, the main novelty of this work is a graphical tool for the design of combustion chambers based on a study of particle trajectory. The program allows one to establish the vertical dimensional limits of the combustion chamber in order to ensure the particles suspension combustion. It is also possible to establish some functional parameters, such as air flow velocity, temperature and fuel ratio, for existing boilers which have fixed dimensions. In such cases, it is important to determine whether the goal is to achieve suspension combustion, or if all the particles in the furnace should be burned, even if some of them burn on the grate.

Acknowledgements

The authors acknowledge the Brazilian research funding agency CNPq and the PEC-PG Program (190560/2012-6) for their financial support of this work. Also, P. L. Curto Risso thanks the Universidad de la República and the SNI program of the Agencia Nacional de Investigación e Innovación (Uruguay) for their support of his research.

References

[1] J.H. Sosa-Arnao, Caldeiras aquatubulares de bagaço-estudo do sistema de recuperação de energia, Ph.D. thesis, Faculdade de Engenharia Mecânica, UNICAMP, 2007.
[2] L. Ma, et al., Modelling the combustion of pulverized biomass in an industrial combustion test furnace, Fuel 86 (12–13) (2007) 1959–1965, http://dx.doi.org/10.1016/j.fuel.2006.12.019.
[3] H. Lu, W. Robert, G. Peirce, B. Ripa, L. Baxter, Comprehensive study of biomass particle combustion, Energy Fuels 22 (4) (2008) 2826–2839, http://dx.doi.org/10.1021/ef800006z.
[4] F. He, F. Behrendt, A new method for simulating the combustion of a large biomass particle a combination of a volume reaction model and front reaction approximation, Combust. Flame 158 (12) (2011) 2500–2511, http://dx.doi.org/10.1016/j.combustflame.2011.04.016.
[5] R. Mehrabian, A. Shiehnejadhesar, R. Scharler, I. Obernberger, Multi-physics modelling of packed bed biomass combustion, Fuel 122 (4) (2014) 164–178, http://dx.doi.org/10.1016/j.fuel.2014.01.027.
[6] Y. Haseli, J. van Oijen, L. de Goey, Reduced model for combustion of a small biomass particle at high operating temperatures, Bioresour. Technol. 131 (2013) 397–404, http://dx.doi.org/10.1016/j.biortech.2012.12.142.
[7] Y. Haseli, J. van Oijen, L. de Goey, A detailed one-dimensional model of combustion of a woody biomass particle, Bioresour. Technol. 102 (20) (2011) 9772–9782, http://dx.doi.org/10.1016/j.biortech.2011.07.075.
[8] P. Woodield, J. Kent, T. Dixon, Computational modelling of combustion instability in bagasse-®red furnaces, Exp. Therm. Fluid Sci. 21 (2000) 17–25.
[9] O. Levenspiel, in: Repla, s. a. (Ed.), Chemical Reaction Engineering, John Wiley and Sons, 1986 (Original edition:.
[10] M. de Souza-Santos, Solid Fuels Combustion and Gasification Modeling, Simulation, and Equipment Operation, Marcel Dekker, New York, 2004.
[11] I. Glassman, R.A. Yetter, Combustion, Elsevier, 2008.

[12] C.D. Blasi, Analysis of convection and secondary reaction effects within porous solid fuels undergoing pyrolysis, Combust. Sci. Technol. 90 (5–6) (1993) 315–340, http://dx.doi.org/10.1080/00102209308907620.
[13] A.K. Sadhukhan, P. Gupta, R.K. Saha, Modelling and experimental studies on pyrolysis of biomass particles, J. Anal. Appl. Pyrolysis 81 (2) (2008) 183–192, http://dx.doi.org/10.1016/j.jaap.2007.11.007.
[14] A. Aboyade, et al., Model fitting kinetic analysis and characterisation of the devolatilization of coal blends with corn and sugarcane residues, Thermochim. Acta 530 (2012) 95–106, http://dx.doi.org/10.1016/j.tca.2011.12.007.
[15] P. Solomon, M. Colket, Coal devolatilization, United Technologies Research Center, East Hartford, Connecticut, 1979, pp. 131–143. Collocquium on coal combustion.
[16] P. Solomon, G. Hamblem, Finding order in coal pyrolysis kinetics, Energy Combust. Sci. 9 (1983) 323–361 doi: http://dx.doi.org/10.1016/0360-1285(83)90012-6.
[17] P. Solomon, et al., General model of coal devolatilization, Energy Fuels 2 (1988) 405–422 doi: http://dx.doi.org/10.1021/ef00010a006.
[18] S. Turns, An Introduction to Combustion: Concept and Applications, McGraw-Hill, Propulsion Engenieering Research Center and Department of Mechanical and Nuclear Engenieering, The Pennsylvania State University, 2000.
[19] J. Saastamoinen, et al., Burnout of pulverized biomass particles in large scale boiler single particle model approach, Biomass Bioenergy 34 (5) (2010) 728–736.
[20] Y.A. Levendis, et al., Combustion behavior in air of single particles from three different coal ranks and from sugarcane bagasse, Combust. Flame 158 (3) (2011) 452–465, http://dx.doi.org/10.1016/j.combustflame.2010.09.007.
[21] M. Momeni, et al., Experimental study on effects of particle shape and operating conditions on combustion characteristics of single biomass particles, Energy fuels 27 (2013) 507–514, http://dx.doi.org/10.1021/ef301343q.
[22] P. Mason, L. Darvell, J. Jones, M. Pourkashanian, A. Williams, Single particle flame-combustion studies on solid biomass fuels, Fuel 151 (2015) 21, http://dx.doi.org/10.1016/j.fuel.2014.11.088.
[23] B. Leckner, Spectral and total emissivity of water vapor and carbon dioxide, Combust. flame 19 (1) (1972) 33–48.
[24] A. Bejan, A.D. Kraus, Heat Transfer Handbook, JOHN WILEY & SONS, INC., United States of America, 2003.
[25] B. Wagenaar, W. Prins, W. van Swaaij, Flash pyrolysis kinetics of pine wood, Fuel Process. Technol. 36 (1–3) (1993) 291–298, http://dx.doi.org/10.1016/0378-3820(93)90039-7.
[26] A. Liden, F. Berruti, D. Scott, A kinetic model for the production of liquids from the flash pyrolysis of biomass, Chem. Eng. Comm. 65 (1) (1988) 207–221, http://dx.doi.org/10.1080/00986448808940254.
[27] I. Milosavljevic, V. Oja, E.M. Suuberg, Thermal effects in cellulose pyrolysis: relationship to char formation processes, Ind. Eng. Chem. Res. 35 (1996) 653–662.
[28] J. Saastamoinen, M. Aho, V. Linna, Simulation pyrolisis and char combustion, Fuel 72 (5) (1993) 599–609.
[29] F. Yi, et al., Three-dimensional time-dependent numerical simulation of a quiescent carbon combustion in air, Fuel 90 (4) (2011) 1522–1528, http://dx.doi.org/10.1016/j.fuel.2010.10.051.
[30] N. Burdine, Relative permeability calculations from pore siza distribution data, Pet. Trans., AIME 198 (3) (1953) 71–78.
[31] S. McBridge, B.J. Gordon, Computer Program for Calculation of Complex Chemial Equlibrium Compositions and Aplication. II. Users Manual and Program Description, vol. 1311, NASA, reference publication, 1996.
[32] P. Lenço, Caracterização do bagaço de cana-de-açúcar para geração de energia, Ph.D. thesis, Faculdade de Engenharia Mecânica, UNICAMP, 2010.
[33] A. Haider, Levenspiel, Drag coefficient and terminal velocity of spherical and nonspherical particles, Powder Technol. 58 (1989) 63–70.
[34] G. Navarrete Cereijo, P. Curto-Risso, W.A. Bizzo, Biomass Particle Suspension Combustion Simulator BPSC-sim, Mendeley Data, v1, 2017, http://dx.doi.org/10.17632/zm7b6npxmz.1.
[35] W. Bizzo, P. Lenço, D. Carvalho, J. Soto Veiga, The generation of residual biomass during the production of bio-ethanol from sugarcane, its characterization and its use in energy production, Renew. Sustain. Energy Rev. 29 (2014) 589–603, http://dx.doi.org/10.1016/j.rser.2013.08.056.
[36] S. Munir, et al., Thermal analysis and devolatilization kinetics of cotton stalk, sugar cane bagasse and shea meal under nitrogen and air atmospheres, Bioresour. Technol. 100 (3) (2009) 1413–1418.